

# The First MAXI/GSC Catalog in the High Galactic-Latitude Sky

Kazuo HIROI,<sup>1</sup> Yoshihiro UEDA,<sup>1</sup> Naoki ISOBE,<sup>1,2</sup> Masaaki HAYASHIDA,<sup>1</sup> Satoshi EGUCHI,<sup>1,3</sup> Mutsumi SUGIZAKI,<sup>4</sup> Nobuyuki KAWAI,<sup>5</sup> Hiroshi TSUNEMI,<sup>6</sup> Masaru MATSUOKA,<sup>4,7</sup> Tatehiro MIHARA,<sup>4</sup> Kazutaka YAMAOKA,<sup>8</sup> Masaki ISHIKAWA,<sup>9</sup> Masashi KIMURA,<sup>6</sup> Hiroki KITAYAMA,<sup>6</sup> Mitsuhiro KOHAMA,<sup>7</sup> Takanori MATSUMURA,<sup>10</sup> Mikio MORII,<sup>5</sup> Yujin E. NAKAGAWA,<sup>11</sup> Satoshi NAKAHIRA,<sup>4</sup> Motoki NAKAJIMA,<sup>12</sup> Hitoshi NEGORO,<sup>13</sup> Motoko SERINO,<sup>4</sup> Megumi SHIDATSU,<sup>1</sup> Tetsuya SOOTOME,<sup>4</sup> Kousuke SUGIMORI,<sup>5</sup> Fumitoshi SUWA,<sup>13</sup> Takahiro TOIZUMI,<sup>5</sup> Hiroshi TOMIDA,<sup>7</sup> Yohko TSUBOI,<sup>10</sup> Shiro UENO,<sup>7</sup> Ryuichi USUI,<sup>5</sup> Takayuki YAMAMOTO,<sup>4</sup> Kyohei YAMAZAKI,<sup>10</sup> Atsumasa YOSHIDA,<sup>8</sup> and the MAXI team

<sup>1</sup>*Department of Astronomy, Kyoto University, Oiwake-cho, Sakyo-ku, Kyoto 606-8502  
hiroii@kusastro.kyoto-u.ac.jp*

<sup>2</sup>*Institute of Space and Astronautical Science (ISAS), Japan Aerospace Exploration Agency (JAXA) ,3-1-1 Yoshino-dai,  
Chuo-ku, Sagamihara, Kanagawa 252-5210*

<sup>3</sup>*National Astronomical Observatory of Japan, 2-21-1, Osawa, Mitaka City, Tokyo 181-8588*

<sup>4</sup>*MAXI team, Institute of Physical and Chemical Research (RIKEN), 2-1 Hirosawa, Wako, Saitama 351-0198*

<sup>5</sup>*Department of Physics, Tokyo Institute of Technology, 2-12-1 Ookayama, Meguro-ku, Tokyo 152-8551*

<sup>6</sup>*Department of Earth and Space Science, Osaka University, 1-1 Machikaneyama, Toyonaka, Osaka 560-0043*

<sup>7</sup>*ISS Science Project Office, Institute of Space and Astronautical Science (ISAS), Japan Aerospace Exploration Agency (JAXA), 2-1-1 Sengen, Tsukuba, Ibaraki 305-8505*

<sup>8</sup>*Department of Physics and Mathematics, Aoyama Gakuin University,  
5-10-1 Fuchinobe, Chuo-ku, Sagamihara, Kanagawa 252-5258*

<sup>9</sup>*School of Physical Science, Space and Astronautical Science, The graduate University for Advanced Studies (Sokendai),  
Yoshinodai 3-1-1, Chuo-ku, Sagamihara, Kanagawa 252-5210*

<sup>10</sup>*Department of Physics, Chuo University, 1-13-27 Kasuga, Bunkyo-ku, Tokyo 112-8551*

<sup>11</sup>*Research Institute for Science and Engineering, Waseda University, 17 Kikui-cho, Shinjuku-ku, Tokyo 162-0044*

<sup>12</sup>*School of Dentistry at Matsudo, Nihon University, 2-870-1 Sakaecho-nishi, Matsudo, Chiba 101-8308*

<sup>13</sup>*Department of Physics, Nihon University, 1-8-14 Kanda-Surugadai, Chiyoda-ku, Tokyo 101-8308*

(Received 2011 June 12; accepted 2011 August 13)

## Abstract

We present the first unbiased source catalog of the Monitor of All-sky X-ray Image (MAXI) mission at high Galactic latitudes ( $|b| > 10^\circ$ ), produced from the first 7-month data (2009 September 1 to 2010 March 31) of the Gas Slit Camera in the 4–10 keV band. We develop an analysis procedure to detect faint sources from the MAXI data, utilizing a maximum likelihood image fitting method, where the image response, background, and detailed observational conditions are taken into account. The catalog consists of 143 X-ray sources above 7 sigma significance level with a limiting sensitivity of  $\sim 1.5 \times 10^{-11}$  ergs cm<sup>-2</sup> s<sup>-1</sup> (1.2 mCrab) in the 4–10 keV band. Among them, we identify 38 Galactic/LMC/SMC objects, 48 galaxy clusters, 39 Seyfert galaxies, 12 blazars, and 1 galaxy. Other 4 sources are confused with multiple objects, and one remains unidentified. The log  $N$  - log  $S$  relation of extragalactic objects is in a good agreement with the HEAO-1 A-2 result, although the list of the brightest AGNs in the entire sky has significantly changed since that in 30 years ago.

**Key words:** catalogs — surveys — galaxies: active — X-rays: galaxies

## 1. INTRODUCTION

All-sky X-ray surveys are powerful tools to investigate the whole populations of active and hot phenomena in the universe at the brightest flux end. The strong X-ray emitters include Galactic objects such as active stars, SNRs, pulsars, CVs, low mass and high mass X-ray binaries (with a neutron star or a black hole as the primary), and extragalactic objects, mainly active galactic nuclei (AGNs; Seyfert galaxies and blazars) and clusters of galaxies. The source catalog consisting of a statistically well-defined sample detected from an unbiased survey is

a primary product on which many subsequent studies are based. For extragalactic populations, in particular, these results define the “local” sample in the present universe, the end point of their cosmological evolution. Thus, to establish the statistical properties of bright X-ray sources using the best quality data over the entire sky has always been a key issue in high energy astrophysics.

Past all-sky X-ray surveys indeed brought valuable information on the X-ray source populations. In the soft X-ray band, the ROSAT mission conducted an all-sky survey in the 0.1–2.4 keV band, producing the ROSAT All-Sky Survey (RASS) Bright Source Catalog (BSC; Voges

et al. 1999) and Faint Source Catalog (FSC; Voges et al. 2000), which contain 18,811 and 105,924 sources, respectively. Because of its large sample size, only a part of the RASS sources has been optically identified (e.g., Schwope et al. 2000). Hard X-rays above 2 keV are more effective to detect obscured objects, such as “type 2” AGNs, due to its strong penetrating power against photoelectric absorption. In the late 1970s, HEAO-1 A-2 performed an all-sky X-ray survey at  $|b| > 20^\circ$  in the 2–10 keV band down to a limiting sensitivity of  $\sim 3.1 \times 10^{-11}$  ergs  $\text{cm}^{-2}$   $\text{s}^{-1}$ , detecting 61 extragalactic sources including 29 AGNs (Piccinotti et al. 1982). *Rossini* X-ray Timing Explorer (RXTE) also carried out an all-sky survey using “slew” mode data of the Proportional Counter Array (PCA) in the 3–8 keV and 8–20 keV bands, and achieved the sensitivity similar to, and an order of magnitude higher than those of HEAO-1 A-1 and A-4, respectively (Revnivtsev et al. 2004). The RXTE/PCA survey detected 294 sources including 100 AGNs, although the identification is not complete (80%). Recently, the Swift and INTEGRAL satellites have performed all-sky surveys in the hard X-ray band above 10 keV (Swift: Tueller et al. 2008; Tueller et al. 2010; Cusumano et al. 2010; Baumgartner et al. 2010, INTEGRAL: Bird et al. 2007; Beckmann et al. 2006, 2009; Krivonos et al. 2007; Bird et al. 2010). These catalogs contain heavily obscured AGNs with absorption column densities larger than  $10^{24}$   $\text{cm}^{-2}$ . Total 628 AGNs have been detected in the Palermo Swift/BAT 54-month catalog (Cusumano et al. 2010).

Monitor of All-sky X-ray Image (MAXI; Matsuoka et al. 2009) is the first scientific mission operated on the international space station (ISS). It carries two types of X-ray cameras: Gas Slit Camera (GSC; Sugizaki et al. 2011; Mihara et al. 2011) and Solid-state Slit Camera (SSC; Tsunemi et al. 2010; Tomida et al. 2011), covering the energy bands of 2–30 keV and 0.5–12 keV, respectively. MAXI/GSC observes nearly the whole sky every 92 minutes with two instantaneous fields of view of  $160^\circ \times 3^\circ$ . One of the main goals of the MAXI mission is to provide a new all-sky X-ray source catalog, including both transient and persistent objects. By integrating the data over a long period, MAXI/GSC is expected to achieve so far the best sensitivities as an all-sky mission that covers the 2–10 keV band (Matsuoka et al. 2009, Ueda et al. 2010). Since its energy band is complementary to that of the RASS (below 2 keV) and to those of Swift/BAT and INTEGRAL (above 10 keV), it will have an advantage in detecting sources having an intrinsically soft continuum with moderate absorption.

In this paper, we present the first MAXI/GSC source catalog detected in the 4–10 keV band at high Galactic latitudes ( $|b| > 10^\circ$ ), utilizing the first 7-month data since the start of its nominal operation. The data reduction and filtering are given in section 2. Section 3 describes the background model of MAXI/GSC used in the analysis and the details of image analysis procedure. In section 4, we present the source catalog and summarize the X-ray properties, results of cross correlation with other catalogs and identification, position accuracy, and  $\log N - \log S$

relations. Section 5 gives the conclusion. The analysis of the local luminosity function of Seyfert galaxies based on this catalog is reported in an accompanying paper (Ueda et al. 2011, submitted to PASJ).

## 2. DATA REDUCTION

For the catalog production, we use the MAXI/GSC data taken between 2009 September 1 and 2010 March 31, when all the GSC counters were operated with a high voltage of 1650 V. Only the data in the 4–10 keV band are utilized in this paper, because in this energy band (1) the energy and position responses are best calibrated at present, and (2) a high signal-to-noise ratio is achieved thanks to high detection efficiency of the counters and to relatively low background rate (Sugizaki et al. 2011).

Starting from the event files with processing version 0.3 provided by the MAXI team, we apply the following data screening to obtain clean data used in the image analysis described in section 3. The processed event files contain columns of the arrival time (TIME), energy (PI), and sky position (R.A. and Dec. ) for each photon as essential information. We utilize the data of all the twelve GSC counters from 2009 September 1 to 22, while those of only eight counters (GSC-0, 1, 2, 3, 4, 5, 7, and 8) are included in the later epoch since the operation of the rest four counters were stopped due to a hardware trouble. The photon events detected by the carbon anodes #1 and #2 in all the counters are excluded because of the response problem in the current calibration. To discard the data suffering from high background rates, we only utilize the data taken when the ISS latitude is between  $-40^\circ$  and  $40^\circ$ , and those detected at the central part of each counter with the photon incident angle  $|\phi| < 38^\circ$  ( $\phi$ ; for definition, see Mihara et al. 2011).

Figure 1 displays the effective exposure map in the Galactic coordinates for the MAXI/GSC 7-month data, where the net exposure corrected for the detection efficiency, multiplied by the projected area of the slit ( $\propto \cos\phi$ ), is given in units of  $\text{s cm}^2$  at each sky position. This is obtained from the simulation utilizing the MAXI simulator **maxisim** (Eguchi et al. 2009) by assuming a uniformly extended emission as the input source; hence this plot is inevitably smoothed by  $\sim 3$  degree, an angular resolution of MAXI.

## 3. ANALYSIS

To detect X-ray sources in an unbiased way from the MAXI/GSC data, we perform an image analysis where the image response, background, and detailed observational conditions are taken into account. We first examine the properties of the MAXI/GSC background on the basis of the on-board data, and attempt to construct a background model (section 3.1). Then, in section 3.2, we employ a two-step approach to search for source candidates, and determine their fluxes and positions.

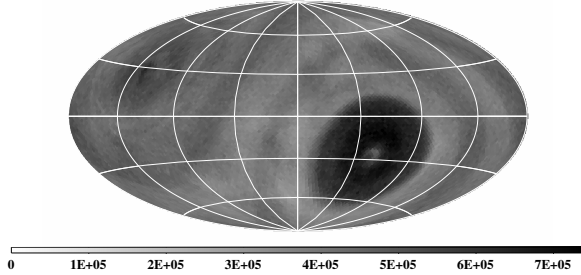


**Fig. 1.** The effective exposure map for the 7-month MAXI/GSC data in the Galactic coordinates projected with the Aitoff algorithm. The unit is  $\text{s cm}^2$ . The black annular-like structures at the bottom-right and top-left positions correspond to regions of the longest exposure near the two poles of the rotation axis of the ISS's orbital motion.

### 3.1. Background Reproduction

In order to securely detect faint X-ray sources with a minimum number of fake detections and to determine their X-ray fluxes precisely, it is of crucial importance to reproduce the instrumental non-X-ray background (NXB) level with a high accuracy. Thus, we model the MAXI/GSC background as a function of time, on the basis of the observational properties. In the case of MAXI, it is difficult to disentangle the cosmic X-ray background (CXB) and NXB from the on-board data, since MAXI rarely observes a direction of the night earth that blocks the CXB. Therefore, we here consider the sum of these two background components.

First, we examine the long-term variability of the background. For this purpose, we make daily averaged background count rate for each counter by rejecting periods when bright X-ray point sources or the bright region along the Galactic plane with  $|l| < 50^\circ$  and  $|b| < 10^\circ$  are within the GSC field of view. We find that the background count rate is significantly different from counter to counter. This is probably due to the difference in the configuration of the counter relative to the ISS and to its direction of orbital motion. Moreover, the background count rate is found to be highly variable on a time scale of days, dependent on the various observational conditions, such as the motion of the solar paddles and the shuttle docking to the ISS.

It is widely known that the short-term variation of the background is tightly correlated with cut-off rigidity (COR) for an X-ray instrument on a low-earth orbit (e.g., Hayashida et al. 1989; Tawa et al. 2008). We confirm such a trend also in the case of MAXI/GSC (Sugizaki et al. 2011), as shown in figure 2, which plots the GSC background count rate against COR of the ISS position. We model this background-COR relation by a third order polynomial, which is shown with the solid line in figure 2.

Utilizing the MAXI simulator (Eguchi et al. 2009), we create background events for the individual counter, with a rate predicted by the background-COR correlation given in figure 2, after the long-term variation is considered. The detector coordinate DETX and the pulse height of each event are randomly assigned in the simulator ac-

ording to the observed distributions of DETX and pulse height, both of which depend on COR (Sugizaki et al. 2011). The simulated event list is then processed in the same way as for the real data, and the sky position in R.A. and DEC. are assigned to each event by referring to the attitude of MAXI and the orbital motion of the ISS.

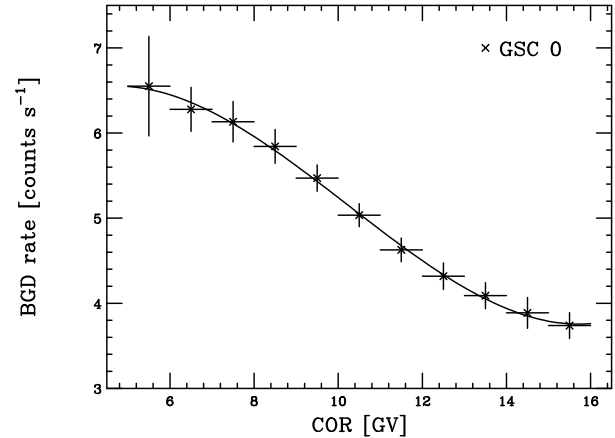


**Fig. 2.** An example of COR dependence of the GSC background count rate for the counter GSC\_0. The peak of the COR-sorted daily-averaged background count rate distribution is plotted, together with its standard deviation.

### 3.2. Image Analysis

Source detection analysis is performed for a tangentially projected image of a small area in the “sky coordinates”, as in the usual case of data analysis of pointing satellites. An image in the sky coordinates,  $(X, Y)$ , is defined by the reference point in R.A. and Dec. corresponding to the image center, the pixel size in units of degree in each direction, and the position angle between the  $+Y$ -axis and the north direction, which is set to be zero in our analysis. The entire sky is divided into 768 square images with a size of  $14^\circ \times 14^\circ$  so that neighboring regions have enough overlapping area with a width of  $>3$  degree in both sides, not to miss any sources near the boundary. The center positions of the images have equal spacing one another, which are adopted from those of the “HEALPix”<sup>1</sup> grid (Górski et al. 2005). Each sky image is produced in the 4–10 keV band from the event list, referring to the columns of energy (PI) and sky position (R.A. and Dec. ). The bin width is set to be 0.1 degree, sufficiently finer than the point spread function of MAXI (Sugizaki et al. 2011).

#### 3.2.1. Step 1: Searching for Source Candidates

For a divided region of the entire sky as noted above, we prepare the images of the real data and simulated background data. The background image is produced on the basis of the model described in section 3.1, by generating 10 times more photons than the actual rate to make the statistical errors negligibly small compared with those in the observed data. By subtracting the background from the data, we obtain the “residual” image. An example of

<sup>1</sup> <http://healpix.jpl.nasa.gov>

the real data is displayed in the left panel of figure 3.

To find source candidates from statistical argument, the data and residual images are smoothed with a circle of  $r = 1^\circ$  with a constant weight of unity (i.e., simple integration). From the integrated counts of the data and residual, we calculate the excess significance at each point as “residual/ $\sqrt{\text{data}}$ ”, thus producing the “significance map” (right panel of figure 3). Then, we search for a peak showing the highest significance in the given image, which is listed as a source candidate if it exceeds  $4\sigma$ . Next, we mask the circular region around its peak position with a radius of 3 degree, where the signals are expected to originate from the same source due to the point spread function. This step is repeated to find another source, which is added to the list of source candidates until the significance of the peak becomes lower than  $4\sigma$ .

In this step, the normalization level of the background profile is estimated from the data themselves for each image, to absorb any remaining systematic errors in reproduction of the background rate, and also to approximately take into account contamination of Galactic diffuse emission in the background. To do this, we first detect bright sources above  $15\sigma$  from the significance map produced by assuming the nominal background rate predicted by the model. Then, after masking out circular regions of  $r = 3^\circ$  around these bright sources, we tune the normalization of the background level so that its total count matches that of the observed data in the same sky region. The tuned level could be slightly overestimated because sources with significances less than  $15\sigma$  are ignored in the first stage. This is not a problem, however, since we set a conservative threshold for picking up the source candidates ( $4\sigma$ ) compared with that for the final catalog ( $7\sigma$ ). Furthermore, as described later (section 3.2.2), we will make iteration of this process to ensure the completeness of the source search by adopting a more accurate background level.

After performing the source search in all the images, we merge the source candidate lists from all of them. In some cases, one source can be independently detected in multiple images, especially when it is located around the edge of the images. We regard any pairs of source candidates whose positional separation is smaller than 1.0 degree are the same object, and we only leave the source detected at the closer position to the image center in the merged list. Further, we also eliminate the source candidates which are regarded as obviously fake detections by visual inspection, such as those detected around a very bright source (like Sco X-1) or over strong extended diffuse emission from a galaxy cluster. We finally have 499 source candidates above  $4\sigma$  at  $|b| > 10^\circ$  in Step 1.

### 3.2.2. Step 2: Determining Flux and Position

As preparation for the image fitting analysis, we construct the point spread function (PSF) model of each source candidate identified in Step 1. We assume that all sources can be treated as point-like in our data. One complexity in the analysis of the MAXI data is that the PSF depends on the position of the detector, and hence its integrated shape in the sky coordinates over multiple orbits is determined by the orbit and attitude condition

of MAXI (Sugizaki et al. 2011). To take this into account, we utilize the MAXI simulator (Eguchi et al. 2009) to construct the PSF model in the sky image under the exactly same conditions as for real data. To suppress the statistical errors in the model, a sufficiently larger number of photons are generated by adopting the Crab Nebula flux (1 Crab) for all source candidates. In the simulation, we choose the same spectrum as the Crab Nebula<sup>2</sup>: an absorbed power law with a photon index of 2.1 and a column density of  $2.6 \times 10^{21} \text{ cm}^{-2}$ . We confirm that the choice of spectrum does not affect the flux determination, even though the PSF also has a weak energy dependence. Comparing the PSF with the data of the brightest point source Sco X-1, we find that the PSF model reproduces the data with residuals corresponding to  $\sim 4\%$  level of the peak height at  $r \sim 1.0$  degree. These systematic errors in the PSF profile do not affect the flux determination of any sources in our catalog that can be regarded as point-like compared with the PSF size.

To determine the flux and position of the source candidates, we perform image fit to the real data in photon count space with a model consisting of the PSFs from the sources and the background. Only the inner region of  $11^\circ \times 11^\circ$  is utilized to ignore the contribution from PSFs of sources located just outside the whole image region of  $14^\circ \times 14^\circ$ . To properly treat statistics with small numbers of photons in each bin, the Poisson maximum likelihood algorithm with MINUIT package (James & Roos 1975) is adopted, based on the so-called  $C$  statistics (Cash 1979), defined as

$$C \equiv 2 \sum_{i,j} \{M(i,j) - D(i,j) \ln M(i,j)\}, \quad (1)$$

where  $D(i,j)$  and  $M(i,j)$  represent the data and model at the image pixel  $(i,j)$ , respectively. The best-fit parameters are obtained by minimizing the  $C$  value, and the  $1\sigma$  statistical error of a single parameter can be estimated by finding that giving the  $C$  value larger by unity than the best-fit. In the fitting process, the normalization of the PSF (i.e., flux) and its position are set to free parameters for all the source candidates, as well as the background level. Figure 4 shows the projection of the left panel of figure 3 onto X-axis (black), superposed with the best-fit model (red: total, blue: background). Since we treat all the sources as point-like, a few bright galaxy clusters may have a small uncertainty in the flux due to their extended structures significantly larger than the PSF (see Note in table 1).

We define the detection significance ( $s_D$ ) of each source as

$$s_D \equiv (\text{best-fit flux}) / (\text{its } 1\sigma \text{ statistical error}). \quad (2)$$

In this paper, we adopt  $s_D > 7$  as the detection criteria for the final catalog, which is conservative enough not to contain any fake detections within current systematic errors in the background model. We verify this by checking the

<sup>2</sup> The spectral parameters are adopted from the INTEGRAL General Reference Catalog (ver. 31). <http://www.isdc.unige.ch/integral/science/catalogue>

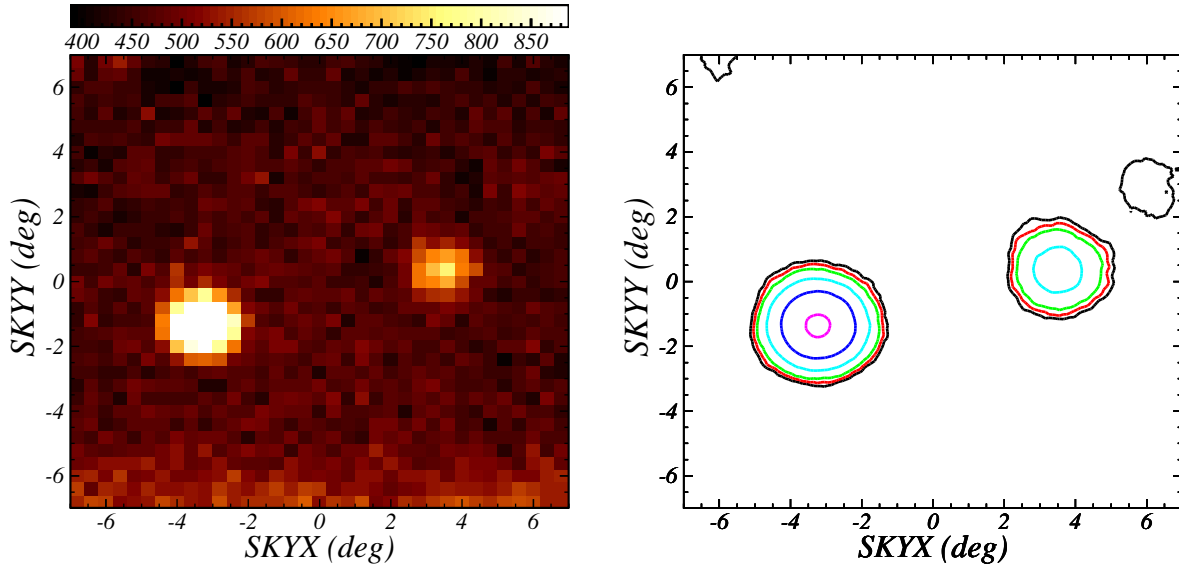


**Fig. 3.** (Left) An example of observed image in photon count space. (Right) The significance map of the same region. The black, red, green, cyan, blue, and purple contours represent the levels of significance of 5, 7, 10, 20, 40, and 70, respectively.

reproducibility of the background profile on a scale of the PSF size ( $\sim 3^\circ$ ) by the following analysis. We search for “negative” signals in the residual image by changing the sign of the significance map in Step 1. Then, we perform image fitting with a model consisting of the background plus negative PSFs identified in the previous step. As a result, it is confirmed that no negative peaks are detected with significances above  $7\sigma$  from all the images. This indicates that the number of fake, positive peaks is also expected to be zero.

Using the tentative source list produced in this way, we repeat the same procedure of Step 1 by applying the best-fit “background plus PSFs” model determined in Step 2, instead of the pure background model as done in the first analysis. The main purpose is to search for missing sources located close to a nearby, brighter source because of the mask around the peak with a radius of 3 degree applied to the significance map in Step 1. Finally, we perform image fitting by adding these newly identified source candidates into the model. The final number of the detected sources with  $s_D > 7$  is 143 at  $|b| > 10^\circ$ , including additional 4 sources found by this iteration process.

The solar paddle structures on the ISS sometimes block a part of the field of view of MAXI, which works to reduce the apparent averaged count rate of an X-ray source. Since we do not take into account these effects in the image analysis, we must evaluate the shielding effect to derive the correct fluxes of the cataloged sources. To estimate it, we perform the whole sky simulations of the CXB with and without the solar paddle occultation during the 7-month period. By comparing these results, we estimate the fraction of unocculted observing time at each sky position. It is found to be  $\approx 96\%$  on average and in a range of 90%–100%, depending on the position. Thus, we correct

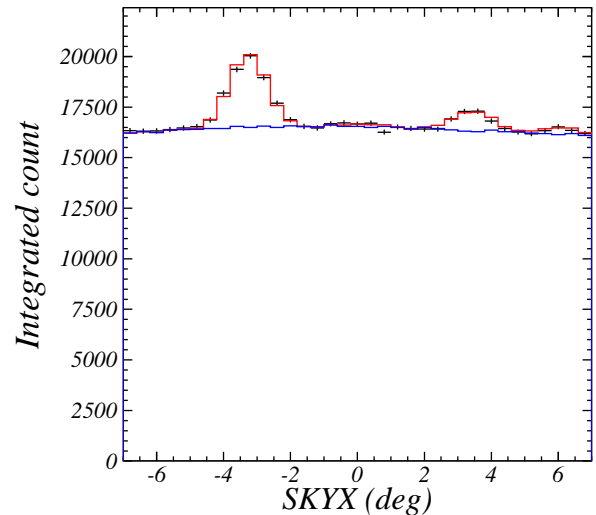


**Fig. 4.** Comparison of the observed data (black) and the best-fit model (red: total, blue: only background). The faintest source in this image is located at  $X = 6.0$  with  $s_D \approx 7$ .

the flux obtained in Step 2 for this fraction according to the sky position, which is finally listed in the catalog.

## 4. MAXI CATALOG

### 4.1. X-Ray Properties

In table 1, we present the first MAXI/GSC catalog at high Galactic latitudes ( $|b| > 10^\circ$ ) compiled from the 7-month data. It contains 143 sources detected with signifi-

cance above  $7s_D$  in the 4–10 keV band, sorted by R.A. and Dec. . The 1st to 7th columns give (1) source identification number, (2) MAXI source name designated from the detected position, (3, 4) MAXI best-fit position in R.A. and Dec., (5) detection significance  $s_D$ , (6) flux in the 4–10 keV band converted from the count rate by assuming a photon index of 2.1, and (7) its  $1\sigma$  statistical error.

The left panel of figure 5 shows the correlation between the detection significance ( $s_D$ ) and the flux. It is seen that  $s_D$  is roughly proportional to the flux in the low flux region where the background determines the noise (statistical fluctuation of photon counts). Whereas in the high flux region, it is proportional to  $(\text{flux})^{1/2}$  since the source photons dominate the noise. The scatter is mainly due to the variation of exposure (see figure 1). The histograms of flux and  $s_D$  are shown in the middle and right panels of figure 5, respectively. The limiting sensitivity is found to be  $\sim 1.2$  mCrab with  $s_D > 7$ , corresponding to  $\sim 1.5 \times 10^{-11}$  ergs  $\text{cm}^{-2}$   $\text{s}^{-1}$  in the 4–10 keV band. This is fully consistent with our expectation from the actual background level and observing efficiency of MAXI (Ueda et al. 2010).

#### 4.2. Identification

Source identification is one of the most important task for the catalog obtained from an unbiased survey. Since the position error of MAXI is typically  $0.4^\circ$  for sources with  $s_D = 7$  at 90% confidence level (section 4.3), direct identification in the optical or near infrared band solely based on the position is practically difficult without further localization. Therefore, we cross correlate our catalog with major X-ray/gamma-ray catalogs for which optical identification or position determination with an  $\sim$ arcsec accuracy is available, assuming that the MAXI sources are likely detected also in these catalogs with similar flux limits. Table 2 lists the catalogs and references we use for the cross correlation; Swift/BAT 58-month and 54-month Catalogs, 1st Fermi/LAT AGN Catalog, the brightest 2200 sources in the 0.5–2 keV band in the RASS BSC, INTEGRAL General Reference Catalog (version 31), NORAS Galaxy Cluster Survey Catalog, REFLEX Galaxy Cluster Survey Catalog, and 1st XMM-Newton Slew Survey Catalog.

To cross correlate the MAXI/GSC catalog with the reference ones, we only take into account the position error of MAXI,  $\sigma_{\text{pos}}$ , since those in the other catalogs are negligibly small. It is defined as

$$\sigma_{\text{pos}} \equiv \sqrt{\sigma_{\text{stat}}^2 + \sigma_{\text{sys}}^2}, \quad (3)$$

where  $\sigma_{\text{sys}}$  is the systematic error of 0.05 degree ( $1\sigma$ , section 4.3) and  $\sigma_{\text{stat}}$  is the statistical one combined from those in the  $X$  and  $Y$  directions at  $1\sigma$  obtained in the image fit process (Step 2). To be conservative, we adopt  $3\sigma_{\text{pos}}$  as the radius for the position matching. We find that this roughly corresponds to a confidence level of 99% in the 2-dimensional space, giving a typical increment in the  $C$  value by 9.2.

The total numbers of possible counterparts found from each reference catalog are also summarized in table 2.

We identify the MAXI sources largely on the basis of this cross-correlation results. Basically, we first look for counterparts in the Swift/BAT and INTEGRAL catalogs, which achieve similar sensitivities to that of MAXI for sources without heavy obscuration. If no sources are found from these catalogs, we also refer to the results with the other catalogs. Ten MAXI sources are found to have no matched counterparts in any of these catalogs within  $3\sigma_{\text{pos}}$ . In such cases, we identify the counterpart by individual inspection using NED<sup>3</sup> and SIMBAD<sup>4</sup>.

To estimate the number of possible spurious identification, we calculate the expected number of coincidental matches between the MAXI sources and those in the reference catalogs,  $N_{\text{cm}}$ , using the following equation:

$$N_{\text{cm}} = \sum_i \rho_i \times S_i, \quad (4)$$

where the suffix  $i$  denotes each reference catalog that can be considered to be independent, and  $\rho_i$  and  $S_i$  are the mean surface number-density of sources in the reference catalog and the total area within the  $3\sigma_{\text{pos}}$  error radii of MAXI sources searched for their counterparts in that catalog, respectively. Here we assume that the spatial distribution of sources in each catalog can be regarded to be random, which is a good approximation in the high Galactic-latitude sky. For simplicity, we only refer to the Swift/BAT 58-month Catalog and the RASS BSC for this calculation, which cover the different energy bands and hence are complementary each other. Following our actual identification procedure, we first consider the Swift/BAT 58-month Catalog and the error region of all MAXI sources, which correspond to  $\rho_1 = 0.022$   $\text{deg}^{-2}$  and  $S_1 = 42$   $\text{deg}^2$ , respectively. Then, to reflect the fact that the remaining MAXI sources without hard X-ray counterparts have been mainly identified by the RASS catalog, we adopt  $\rho_2 = 0.054$   $\text{deg}^{-2}$  for the 1829 brightest RASS sources and  $S_2 = 18$   $\text{deg}^2$  for the MAXI error regions. In this way, we obtain  $N_{\text{cm}} = 1.9$ . Note that this is a conservative estimate since we have neglected the duplicative sources between the Swift/BAT and RASS catalogs in the calculation.

Out of the total 143 MAXI sources, we finally identify 142 sources, and only one source<sup>5</sup> remains unidentified. The locations of the cataloged sources are plotted in figure 6 in the Galactic coordinates with different colors corresponding to different types of object. Table 3 gives a summary of source identification. The catalog contains 38 Galactic/LMC/SMC objects, 48 galaxy clusters, 51 AGNs including 12 blazars. The detailed information of the counterparts is provided in the 8th to 14th columns of table 1 for each MAXI source, (8) the source name, (9, 10) the position of the counterpart in R.A. and Dec., (11) type, (12) redshift (only for extragalactic objects), (13) other names of the source, and (14) notes in special cases. We find four MAXI sources<sup>6</sup> are probably confused from

<sup>3</sup> <http://ned.ipac.caltech.edu>

<sup>4</sup> <http://simbad.u-strasbg.fr/simbad>

<sup>5</sup> MAXI J0457–696

<sup>6</sup> MAXI J0627–540, J0957+693, J1633–750, and J1941–104

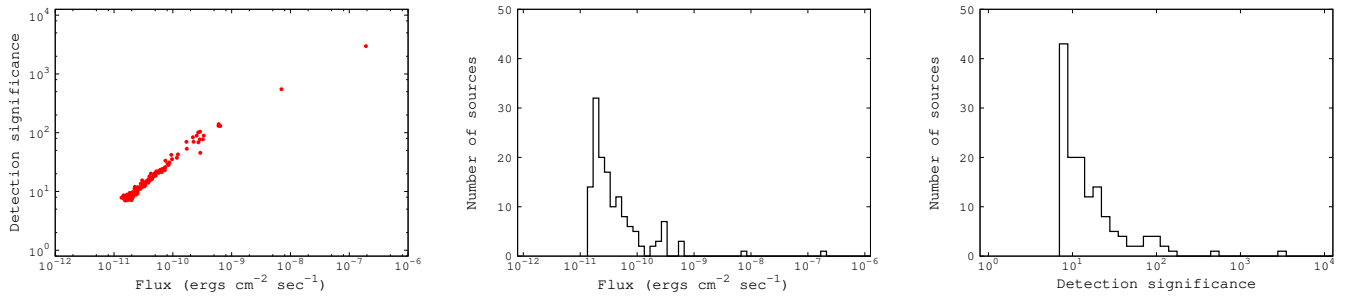


**Fig. 5.** The correlation between the detection significance and the flux for all the sources in the MAXI/GSC catalog (left), the distribution of the flux (middle), and that of the detection significance (right).

**Table 2.** Reference catalogs used for cross correlation.

Catalog	Number of matched sources	Reference
Swift/BAT 58-month Catalog	93	Baumgartner et al. 2010*
54-month Palermo BAT-Survey Catalog (2PBC)	100	Cusumano et al. 2010
1st Fermi/LAT AGN Catalog (1LAC)	12	Abdo et al. 2010
RASS Bright Souce Catalog (1RXS)	110	Voges et al. 1999
INTEGRAL General Reference Catalog (ver. 31)	108	INTEGRAL Science Data Centre website <sup>†</sup>
NORAS Galaxy Cluster Survey Catalog	14	Böhringer et al. 2000
REFLEX Galaxy Cluster Survey Catalog	17	Böhringer et al. 2004
1st XMM-Newton Slew Survey Catalog (XMMSL1)	65	Saxton et al. 2008

\* The data is retrieved from NASA website: <http://heasarc.nasa.gov/docs/swift/results/bs58mon>

<sup>†</sup> <http://www.isdc.unige.ch/integral/science/catalogue>

multiple objects that are difficult to be resolved with the angular resolution of MAXI. For those sources, multiple counterparts are listed in table 1, which are not counted in the identification summary shown in table 3.

We compare the number statistics of source populations in the first MAXI/GSC catalog with those in the HEAO-1 A-2 ( $|b| > 20^\circ$ , Piccinotti et al. 1982), RXTE ( $|b| > 10^\circ$ , Revnivtsev et al. 2004), and Swift/BAT (Cusumano et al. 2010) catalogs. The number ratios between Galactic objects, AGNs, and galaxy clusters in our catalog, 21:40:36 ( $|b| > 20^\circ$ ) and 38:51:48 ( $|b| > 10^\circ$ ), are found to be consistent with both HEAO-1 A-2 (17:29:30) and RXTE (63:100:64) results within the statistical errors. By contrast, the Swift/BAT survey performed in the 15–150 keV band brings a significantly higher fraction of AGNs at  $|b| > 10^\circ$ ,  $\sim 60\%$ , than these catalogs produced in lower energy bands. We confirm that all but two galaxy clusters in the HEAO-1 A-2 catalog are listed in ours, with the remaining two also detected with slightly lower significances than  $s_D = 7$  in the MAXI/GSC data. We note, however, that about 40% ( $= 12/29$ ) of the Piccinotti AGNs are absent in our catalog. In fact, the X-ray fluxes of these 12 AGNs obtained from pointing observations with ASCA, XMM-Newton, or Swift/XRT in more recent years (Winter et al. 2009, Shinozaki et al. 2006, Aharonian et al. 2005, and Blustin et al. 2004) are all lower than the typical limiting sensitivity of the MAXI survey,  $\approx 2 \times 10^{-11}$

**Table 3.** Categories of cataloged sources.

Category	Number of sources
unidentified	1
galaxies	1
galaxy clusters	48
Seyfert galaxies	39
blazars	12
CVs/Stars	20
X-ray binaries	18
confused	4

ergs  $\text{cm}^{-2} \text{s}^{-1}$  in the 4–10 keV band (figure 9, in section 4.4), by assuming a power law photon index of 2. This fact indicates that the list of the brightest X-ray AGNs in the whole sky has significantly changed since  $\sim 30$  years ago due to their long-term variability.

#### 4.3. Position Accuracy

Utilizing the source identification result, we estimate the positional error of MAXI as a function of the detection significance, which is observationally determined. Therefore, it gives the most robust information useful for identification work of MAXI sources within the current calibration. Figure 7 shows the source distributions as a

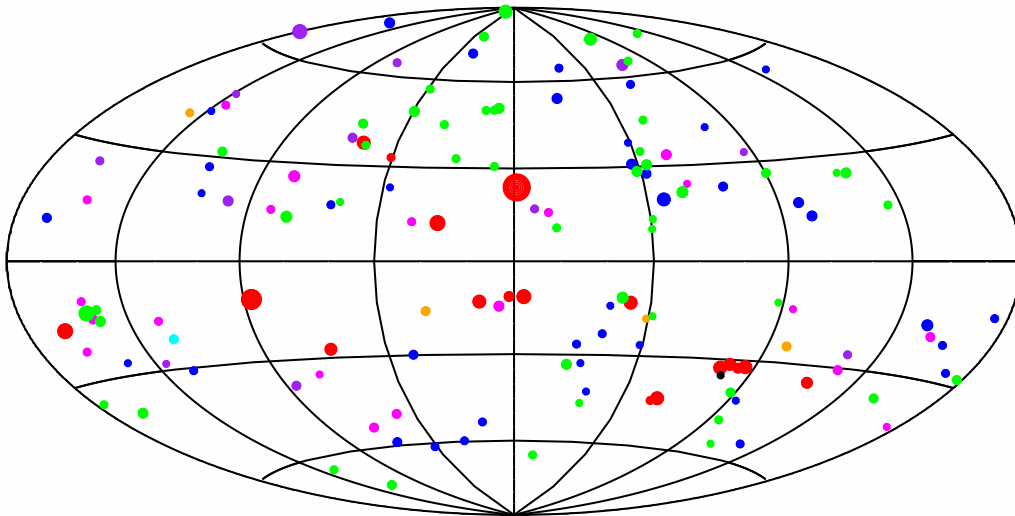


**Fig. 6.** Locations of cataloged sources with  $s_D > 7$  in the Galactic coordinates. The radius is proportional to logarithm of the 4–10 keV flux. Different colors correspond to different types of sources: unidentified (black); galaxies (cyan); galaxy clusters (green); Seyfert galaxies (blue); blazars (purple); CVs/Stars (magenta); X-ray binaries (red); and confused (orange).

function of the angular separation between the MAXI position and that of the counterpart in different  $s_D$  ranges;  $s_D = 7 - 10$  (left),  $s_D = 10 - 30$  (middle), and  $s_D > 30$  (right). From each distribution, we measure a 90% error radius by counting the number of sources.

Figure 8 plots the 90% error radius as a function of the detection significance. In the highest  $s_D$  bin, the statistical errors are expected to be negligibly small compared with the systematic errors due to those in the attitude determination and position calibration of the GSC (Sugizaki et al. 2011). We thus estimate the systematic error to be  $\sigma_{\text{sys}}^{90} \sim 0.08$  degree (90% confidence level), or  $\sigma_{\text{sys}} \sim 0.05$  degree ( $1\sigma$ ). In the lower significance region, the total error is dominated by the statistical error, which is expected to be proportional to  $s_D^{-1}$ . We obtain the best-fit formula for the 90% positional error of MAXI sources

$$\sigma_{\text{pos}}^{90}(s_D) = \sqrt{(A/s_D)^2 + (\sigma_{\text{sys}}^{90})^2}, \quad (5)$$

where  $A = 3.08 \pm 0.04$  and  $\sigma_{\text{sys}}^{90} = 0.08$ .

#### 4.4. $\log N - \log S$ Relation

Source number counts ( $\log N - \log S$  relation) give the most fundamental statistical properties of source populations that can be derived from survey observations. To obtain this, we need to have an area curve, where survey area guaranteed for detection of a source with the given detection criteria (i.e.,  $s_D > 7$ ) is given as a function of flux. We estimate the sensitivities at each sky position from (1) the background photon counts and (2) the product of effective detector area  $\times$  exposure obtained from the CXB simulation (shown in figure 1). We confirm that the actual detection significance derived from the PSF fit can be well approximated by that analytically calculated

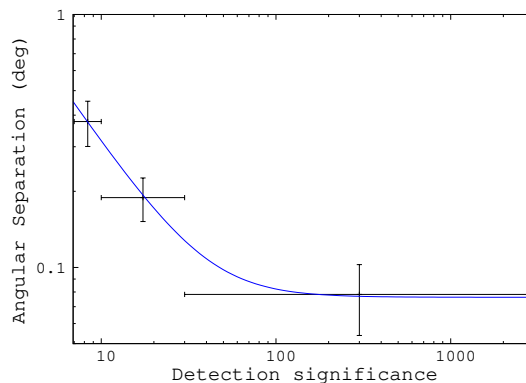


**Fig. 8.** 90% error radius of MAXI sources plotted as a function of the detection significance. The blue curve indicates the best-fit formula with the form of  $\sqrt{(3.08/s_D)^2 + (0.08)^2}$  (degree).

from these parameters on the basis of a simple statistical argument. Figure 9 plots the area curve calculated in this way; we confirm that the  $7\sigma$  sensitivity is  $\approx 1.2$  mCrab, or  $1.5 \times 10^{-11}$  ergs  $\text{cm}^{-2}$   $\text{s}^{-1}$ , in the 4–10 keV band.

Dividing the flux distribution of the detected sources by the survey area gives  $\log N - \log S$  relation in the differential form. Figure 10 shows that in the integral form, where the source number density  $N$  above flux  $S$  is plotted. We separately plot those of all the sources and extragalactic objects. The results for extragalactic objects are in an excellent agreement with the HEAO-1 A-2 result by Piccinotti et al. 1982, by converting the fluxes from the 2–10 keV band into the 4–10 keV band assuming a photon

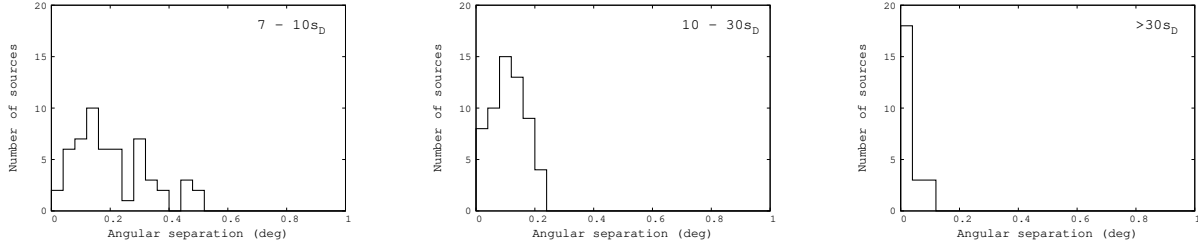


**Fig. 7.** Source distributions as a function of the angular separation between the MAXI position and that of the counterpart for different regions of detection significance (from left to right,  $7-10s_D$ ,  $10-30s_D$ , and  $>30s_D$ ).

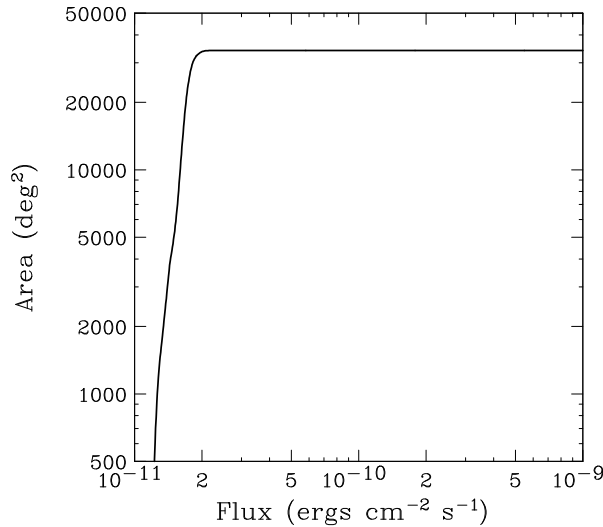


**Fig. 9.** Area curve of the 7-month MAXI/GSC survey at  $|b| > 10^\circ$  in the 4–10 keV band, for the detection significance of  $s_D > 7$ .

index of 2. We recall, however, that the actual content of the AGN sample has been significantly changed since the HEAO-1 A2 era, as mentioned in section 4.2.

## 5. CONCLUSION

We present the first MAXI/GSC catalog produced from an unbiased X-ray survey in the 4–10 keV band at high Galactic latitude sky ( $|b| > 10^\circ$ ). The initial 7-month data after the start of normal operation are utilized here. The limiting sensitivity of  $1.5 \times 10^{-11}$  ergs  $\text{cm}^{-2}$   $\text{s}^{-1}$  (1.2 mCrab) is achieved for the detection significance criteria of  $> 7s_D$ , which is conservatively adopted in this paper not to contain fake sources under the current calibration. The sensitivity already exceeds that of the HEAO-1 A-2 all-sky survey in the 2–10 keV band. It is expected to be improved significantly by adding more data and by further improvement of the background model calibration.

The catalog contains 143 sources, which are identified as 38 Galactic/LMC/SMC objects, 48 galaxy clusters, 39 Seyferts, 12 blazars, 1 galaxy, and 4 confused objects. Only one source remains unidentified. The high completeness of this catalog makes it particularly useful to investi-

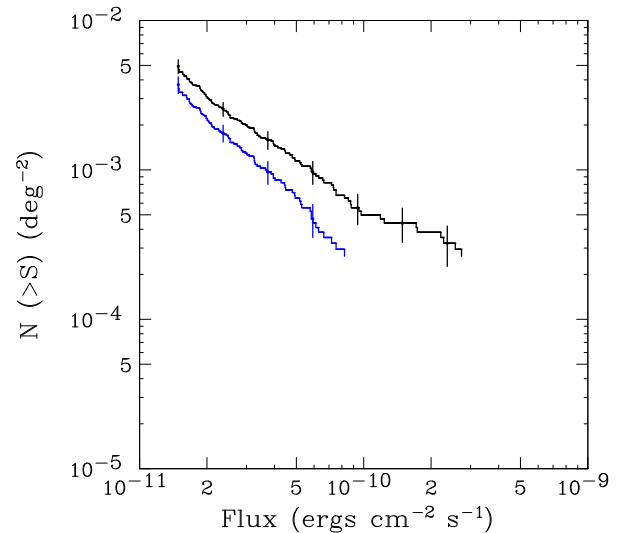


**Fig. 10.** Log  $N$  - log  $S$  relations in the 4–10 keV band obtained from the 7-month MAXI/GSC survey at  $|b| > 10^\circ$ . From top to bottom, those of the total sources (black) and extragalactic objects (blue). The error bars correspond to the 90% statistical errors in the source counts.

gate the statistical properties of X-ray populations in the local universe with the least uncertainties. The initial results on the X-ray luminosity function of Seyfert galaxies are reported in the accompanying paper.

This research has made use of the NASA/IPAC Extragalactic Database (NED) which is operated by the Jet Propulsion Laboratory, California Institute of Technology, under contract with the National Aeronautics and Space Administration. This research has made use of the SIMBAD database, operated at CDS, Strasbourg, France. Some of the results in this paper have been derived using the HEALPix (K.M. Górski et al., 2005, ApJ, 622, p759) package. This research was partially supported by the Ministry of Education, Culture, Sports, Science and Technology (MEXT), Grant-in-Aid No.19047001, 20041008, 20244015, 20540237, 21340043, 21740140, 22740120, 23000004, 23540265, and Global-COE from MEXT “The Next Generation of Physics, Spun from Universality and Emergence” and “Nanoscience and Quantum Physics”.

## References

- Abdo, A. A., et al. 2010, *ApJ*, 715, 429
- Aharonian, F., et al. 2005, *A&A*, 442, 895
- Baumgartner, W. H., et al. 2010, *ApJS*, submitted
- Beckmann, V., Gehrels, N., Shrader, C. R., & Soldi, S. 2006, *ApJ*, 638, 642
- Beckmann, V., et al. 2009, *A&A*, 505, 417
- Bird, A. J., et al. 2007, *ApJS*, 170, 175
- Bird, A. J., et al. 2010, *ApJS*, 186, 1
- Blustin, A. J., Page, M. J., & Branduardi-Raymont, G. 2004, *A&A*, 417, 61
- Böhringer, H., et al. 2000, *ApJS*, 129, 435
- Böhringer, H., et al. 2004, *A&A*, 425, 367
- Cash, W. 1979, *ApJ*, 228, 939
- Cusumano, G., et al. 2010, *A&A*, 524, A64
- Eguchi, S., Hiroi, K., Ueda, Y., Sugizaki, M., Tomida, H., Suzuki, M., & The Maxi Team 2009, *Astrophysics with All-Sky X-Ray Observations*, 44
- Górski, K. M., Hivon, E., Banday, A. J., Wandelt, B. D., Hansen, F. K., Reinecke, M., & Bartelmann, M. 2005, *ApJ*, 622, 759
- Guainazzi, M., Piconcelli, E., Jiménez-Bailón, E., & Matt, G. 2005, *A&A*, 429, L9
- Hayashida, K., Inoue, H., Koyama, K., Awaki, H., Takano, S., 1989, *PASJ*, 41, 373
- Isobe, N., et al. 2010, *PASJ*, 62, L55
- James, F., & Roos, M. 1975, *Computer Physics Communications*, 10, 343
- Krivonos, R., Revnivtsev, M., Lutovinov, A., Sazonov, S., Churazov, E., & Sunyaev, R. 2007, *A&A*, 475, 775
- Matsumura, T., et al. 2011, *The Astronomer's Telegram*, 3308, 1
- Matsuoka, M., et al. 2009, *PASJ*, 61, 999
- Mihara, T., et al. 2011, *PASJ*, in press
- Piccinotti, G., Mushotzky, R. F., Boldt, E. A., Holt, S. S., Marshall, F. E., Serlemitsos, P. J., & Shafer, R. A. 1982, *ApJ*, 253, 485
- Revnivtsev, M., Sazonov, S., Jahoda, K., & Gilfanov, M. 2004, *A&A*, 418, 927
- Saxton, R. D., Read, A. M., Esquej, P., Freyberg, M. J., Altieri, B., & Bermejo, D. 2008, *A&A*, 480, 611
- Schwöpe, A., et al. 2000, *Astronomische Nachrichten*, 321, 1
- Sekiguchi, K., & Wolstencroft, R. D. 1992, *MNRAS*, 255, 581
- Shinozaki, K., Miyaji, T., Ishisaki, Y., Ueda, Y., & Ogasaka, Y. 2006, *AJ*, 131, 2843
- Sugizaki, M., et al. 2011, *PASJ*, in press
- Suzuki, M., et al. 2010, *The Astronomer's Telegram*, 2401, 1
- Tawa, N., et al., 2008, *PASJ*, 60, S11
- Tomida, H., et al. 2011, arXiv:1101.3651
- Tsunemi, H., Tomida, H., Katayama, H., Kimura, M., Daikyūji, A., Miyaguchi, K., Maeda, K., & MAXI Team 2010, *PASJ*, 62, 1371
- Tueller, J., Mushotzky, R. F., Barthelmy, S., Cannizzo, J. K., Gehrels, N., Markwardt, C. B., Skinner, G. K., & Winter, L. M. 2008, *ApJ*, 681, 113
- Tueller, J., et al. 2010, *ApJS*, 186, 378
- Ueda, Y., Hiroi, K., Isobe, N., Hayashida, M., Sugizaki, M., & Maxi Team 2010, *The First Year of MAXI: Monitoring Variable X-ray Sources*, 4th International MAXI Workshop held November 30 – December 2, 2010 in Tokyo, Japan
- Voges, W., et al. 1999, *A&A*, 349, 389
- Voges, W., et al. 2000, *IAU Circ.*, 7432, 3
- Winter, L. M., Mushotzky, R. F., Reynolds, C. S., & Tueller, J. 2009, *ApJ*, 690, 1322

Table 1. Cataloged sources in the MAXI/GSC survey.

(1) No.	(2) MAXI Name	(3) MAXI R.A.	(4) MAXI Decl.	(5) Significance	(6) Flux <sup>a</sup>	(7) Error <sup>a</sup>	(8) Counterpart Name	(9) Ctpt. R.A.	(10) Ctpt. Decl.	(11) Type <sup>b</sup>	(12) Redshift <sup>c</sup>	(13) Other Name	(14) Note <sup>d</sup>
1	MAXI J0042-093	10.5	-9.4	16.2	4.4	0.3	Abell 85	10.408	-9.342	Galaxy Cluster	0.05506	4U 0037-10	
2	MAXI J0043+410	10.8	41.1	16.0	3.9	0.2	M31	10.678	41.179	Galaxy		Andromeda Galaxy	
3	MAXI J0048+320	12.1	32.0	10.4	2.4	0.2	Mrk 348	12.196	31.957	Sy2	0.01503	2E 0046.0+3140	
4	MAXI J0053-726	13.4	-72.7	15.5	3.0	0.2	2E 0050.1-7247	12.972	-72.530	HMXB			
5	MAXI J0055+462	13.8	46.3	8.3	1.9	0.2	1RXS J005528.0+461143	13.867	46.195	CV/DQ Her		SWIFT J0055.4+4612	
6	MAXI J0056-012	14.2	-1.3	8.6	2.1	0.2	Abell 119	14.089	-1.263	Galaxy Cluster	0.0442	4U 0050-01	
7	MAXI J0117-734	19.3	-73.4	103.9	29.0	0.3	SMC X-1	19.271	-73.443	HMXB/NS		3A 0116-736, 4U 0115-73	
8	MAXI J0125+341	21.3	34.1	7.0	1.5	0.2	1ES 0120+340	20.786	34.347	BL Lac	0.272	1ES 0120+34.0	
9	MAXI J0229+315	37.4	31.6	8.1	1.8	0.2	NGC 931	37.060	31.312	Sy1.5	0.01665	1ES 0225+31.0	
10	MAXI J0254+416	43.7	41.6	22.8	5.9	0.2	WBL 088	43.634	41.586	Galaxy Cluster	0.017239	4U 0253+41	
11	MAXI J0258+133	44.7	13.4	19.6	4.9	0.2	Abell 401	44.737	13.582	Galaxy Cluster	0.0748	2E 0256.2+1322	
12	MAXI J0301+443	45.3	44.3	13.1	3.3	0.2	CIZA J0300.7+4427	45.188	44.463	Galaxy Cluster	0.03	XSS J03008+4429	
13	MAXI J0308+409	47.0	41.0	17.7	4.6	0.2	Algol	47.042	40.958	Algol Type Eclipsing binary		2E 0304.9+4045	(A)
14	MAXI J0317-443	49.3	-44.4	7.2	1.9	0.3	Abell 3112	49.494	-44.239	Galaxy Cluster	0.075252	1ES 0316-44.4	
15	MAXI J0319+415	50.0	41.5	130.9	59.7	0.4	Perseus Cluster	49.951	41.512	Galaxy Cluster	0.01756	4U 0316+41	(B)
16	MAXI J0327+288	51.8	28.8	8.7	1.9	0.2	UX Ari	51.646	28.717	RS CVn		3A 0322+277	(C)
17	MAXI J0331+437	52.8	43.8	9.4	2.3	0.2	GK Per	52.799	43.905	CV/DQ Her		3A 0327+438	
18	MAXI J0333-364	53.3	-36.4	7.8	2.0	0.2	NGC 1365	53.402	-36.140	Sy1.8	0.00546	2E 0331.7-3618	
19	MAXI J0337+004	54.3	0.5	7.9	1.9	0.2	HR 1099	54.197	0.588	RS CVn		4U 0336+01	(D)
20	MAXI J0339+099	54.8	10.0	10.3	2.5	0.2	ZwCl 0335+0956	54.647	9.965	Galaxy Cluster	0.0349	4U 0344+11	
21	MAXI J0343-537	55.9	-53.8	10.9	2.3	0.2	Abell 3158	55.665	-53.631	Galaxy Cluster	0.0597	4U 0339-54	
22	MAXI J0355+310	58.9	31.1	139.9	60.2	0.4	X Per	58.846	31.046	HMXB/NS		4U 0352+30, 4U 0352+309	
23	MAXI J0413+105	63.4	10.5	18.7	4.7	0.2	Abell 478	63.336	10.476	Galaxy Cluster	0.0881	4U 0410+10	
24	MAXI J0423-569	65.9	-56.9	8.1	1.7	0.2	1RXS J042601.6-571202	66.503	-57.200	Sy1.5	0.104		
25	MAXI J0431-613	68.0	-61.4	20.1	4.2	0.2	Abell 3266	67.800	-61.406	Galaxy Cluster	0.0589	4U 0427-61	
26	MAXI J0433+053	68.4	5.3	11.7	2.8	0.2	3C 120	68.296	5.354	Sy1	0.03301	4U 0432+05	
27	MAXI J0433-131	68.5	-13.2	15.3	3.6	0.2	Abell 496	68.308	-13.259	Galaxy Cluster	0.0329	4U 0431-12	
28	MAXI J0457-696	74.5	-69.7	8.1	1.5	0.2	UNKNOWN						
29	MAXI J0510+166	77.7	16.7	11.5	2.8	0.2	IRAS 05078+1626	77.690	16.499	Sy1.5	0.01788	4U 0517+17	
30	MAXI J0514-400	78.5	-40.1	37.5	11.7	0.3	NGC 1851	78.528	-40.044	LMXB/NS in globular c			
31	MAXI J0516-001	79.1	-0.2	9.4	2.2	0.2	Ark 120	79.048	-0.150	Sy1	0.0323	H 0523-00	
32	MAXI J0520-719	80.1	-71.9	100.9	27.0	0.3	LMC X-2	80.117	-71.965	LMXB		4U 0520-72	
33	MAXI J0529-327	82.3	-32.7	15.5	4.1	0.3	TV Col	82.356	-32.818	CV/DQ Her		3A 0527-329	
34	MAXI J0533-662	83.3	-66.3	33.5	7.5	0.2	LMC X-4	83.207	-66.371	HMXB/NS		4U 0532-66, 4U 0532-664	
35	MAXI J0535-054	83.8	-5.5	18.2	4.8	0.3	Trapezium Cluster	83.819	-5.387	Star Cluster		1ES 0532-05.4	
36	MAXI J0539-640	84.8	-64.1	89.0	25.4	0.3	LMC X-3	84.734	-64.082	HMXB/BHC		4U 0538-64	
37	MAXI J0539-696	85.0	-69.6	69.9	17.0	0.2	LMC X-1	84.911	-69.743	HMXB/BHC		4U 0540-69	
38	MAXI J0542+606	85.7	60.7	11.3	2.5	0.2	BY Cam	85.704	60.859	CV/AM Her		4U 0541+60	
39	MAXI J0550-322	87.6	-32.2	8.3	2.1	0.2	PKS 0548-322	87.670	-32.272	BL Lac	0.069	4U 0543-31	
40	MAXI J0552-075	88.1	-7.5	29.6	8.1	0.3	NGC 2110	88.047	-7.456	Sy2	0.00779	1H 0551-074	
41	MAXI J0555+464	88.8	46.5	15.1	3.7	0.2	MCG +08-11-011	88.723	46.439	Sy1.5	0.02048	4U 0558+46	
42	MAXI J0627-540	96.8	-54.0	14.4	3.2	0.2	ABELL 3391	96.564	-53.681	Galaxy Cluster	0.0531	1ES 0625-53.6	
"	"	"	"	"	"	"	ABELL 3395	96.879	-54.399	Galaxy Cluster	0.0498	1E 0626.2-5428	
43	MAXI J0710+590	107.7	59.1	9.0	2.1	0.2	QSO B0706+591	107.625	59.139	BL Lac	0.125	1H 0658+595	
44	MAXI J0744-532	116.1	-53.3	7.5	1.6	0.2	V0436 Car	116.243	-52.952	CV/DQ Her		RX J0744.9-5257	

Table 1 (cont'd)

(1) No.	(2) MAXI Name	(3) MAXI R.A.	(4) MAXI Decl.	(5) Significance	(6) Flux <sup>a</sup>	(7) Error <sup>a</sup>	(8) Counterpart Name	(9) Ctpt. R.A.	(10) Ctpt. Decl.	(11) Type <sup>b</sup>	(12) Redshift <sup>c</sup>	(13) Other Name	(14) Note <sup>d</sup>
45	MAXI J0814-572	123.7	-57.3	9.4	1.9	0.2	CIZA J0812.5-5714	123.126	-57.235	Galaxy Cluster	0.062		
46	MAXI J0817-074	124.3	-7.5	9.6	2.5	0.3	Abell 644	124.356	-7.517	Galaxy Cluster	0.0704	2A 0815-075	
47	MAXI J0909-097	137.4	-9.7	21.3	5.8	0.3	Abell 754	137.209	-9.637	Galaxy Cluster	0.0542	4U 0900-09	
48	MAXI J0918-121	139.6	-12.2	7.2	1.7	0.2	Abell 780	139.527	-12.093	Galaxy Cluster	0.0539	1H 0917-121	
49	MAXI J0924-317	141.0	-31.7	21.2	5.8	0.3	6dFGS gJ092353.7-314131	140.974	-31.692	Sy1.9	0.04225	SWIFT J0924.2-3141	
50	MAXI J0947-309	146.9	-31.0	24.1	6.6	0.3	MCG -05-23-016	146.917	-30.949	Sy2	0.00849	4U 0945-30	
51	MAXI J0957+693	149.3	69.4	11.2	2.2	0.2	M81	148.888	69.065	Galaxy			
"	"	"	"	"	"	"	M82	148.970	69.679	Galaxy		4U 1004+70	
"	"	"	"	"	"	"	1RXSJ095755.0+690310	149.472	69.063	ULX		1E 0953.8+6918	
52	MAXI J1023+197	155.8	19.8	8.0	1.8	0.2	NGC 3227	155.877	19.865	Sy1.5	0.00386	3A 1021+203	
53	MAXI J1036-276	159.2	-27.6	13.0	3.2	0.2	Abell 1060	159.214	-27.526	Galaxy Cluster	0.0126	4U 1033-26	
54	MAXI J1104-235	166.0	-23.5	7.2	1.6	0.2	1ES 1101-232	165.907	-23.492	BL Lac	0.186	4U 1057-21	
55	MAXI J1104+382	166.1	38.2	89.3	33.5	0.3	Mrk 421	166.114	38.209	BL Lac	0.03002	3A 1102+385	(E)
56	MAXI J1105+725	166.3	72.5	9.2	1.8	0.2	NGC 3516	166.698	72.569	Sy1.5	0.00884	1E 1103.4+7250	
57	MAXI J1135+676	174.0	67.6	7.5	1.5	0.2	RGB J1136+676	174.125	67.618	BL Lac	0.13423	RX J1136.5+6737	
58	MAXI J1139-378	174.9	-37.8	12.3	3.2	0.3	NGC 3783	174.757	-37.739	Sy1	0.00973	4U 1136-37	
59	MAXI J1141+715	175.4	71.5	9.8	2.1	0.2	DO Dra	175.910	71.689	CV/DQ Her		3A 1148+719	
60	MAXI J1144+198	176.2	19.8	11.8	2.7	0.2	Abell 1367	176.186	19.700	Galaxy Cluster	0.022	4U 1143+19	
61	MAXI J1144-184	176.2	-18.4	8.4	1.9	0.2	2MASX J11454045-1827149	176.419	-18.454	Sy1	0.03295	1A 1143-18	
62	MAXI J1210+394	182.6	39.4	23.4	6.2	0.2	NGC 4151	182.636	39.406	Sy1.5	0.00332	4U 1206+39	
63	MAXI J1218+038	184.7	3.8	8.0	2.0	0.2	ZwCl 1215.1+0400	184.419	3.662	Galaxy Cluster	0.075	1RXS J121742.6+033943	
64	MAXI J1229+020	187.3	2.0	30.3	8.7	0.3	3C 273	187.278	2.052	Blazar	0.15834	4U 1226+02	
65	MAXI J1230+124	187.6	12.4	53.3	17.2	0.3	Virgo galaxy cluster	187.706	12.391	Galaxy Cluster	0.00436	H 1228+125	(B)
66	MAXI J1237-386	189.4	-38.6	7.4	1.8	0.3	V1025 Cen	189.569	-38.712	CV/DQ Her		RX J1238.2-3842	
67	MAXI J1240-052	190.1	-5.3	7.8	2.0	0.3	NGC 4593	189.914	-5.344	Sy1	0.009	4U 1240-05	
68	MAXI J1249-413	192.3	-41.3	28.2	8.4	0.3	Abell 3526	192.216	-41.306	Galaxy Cluster	0.0114	4U 1246-41	
69	MAXI J1252-292	193.2	-29.3	24.3	7.3	0.3	EX Hya	193.102	-29.249	CV/DQ Her		4U 1249-28	
70	MAXI J1258-176	194.5	-17.6	8.7	2.1	0.2	Abell 1644	194.311	-17.354	Galaxy Cluster	0.0473	3A 1254-171	
71	MAXI J1259+279	194.9	28.0	70.1	22.5	0.3	Coma Cluster	194.953	27.981	Galaxy Cluster	0.0231	4U 1257+28	(B)
72	MAXI J1325-430	201.4	-43.0	76.8	28.7	0.4	Cen A	201.365	-43.019	Sy2	0.00183	4U 1322-42	
73	MAXI J1327-272	201.9	-27.2	7.7	1.9	0.2	Abell 1736	202.084	-27.299	Galaxy Cluster	0.0458	1H 1326-269	
74	MAXI J1328-315	202.2	-31.6	18.7	5.1	0.3	Abell 3558	201.990	-31.503	Galaxy Cluster	0.048	1ES 1325-31.2	
75	MAXI J1335-342	203.9	-34.3	13.7	3.4	0.2	MCG -06-30-015	203.974	-34.296	Sy1.2	0.00775	H 1332-336	
76	MAXI J1336-237	204.0	-23.8	7.1	1.7	0.2	ESO 509-IG66	203.668	-23.446	Sy2	0.03431	IRAS 13319-2311	(F)
77	MAXI J1338+045	204.6	4.6	11.8	2.9	0.2	NGC 5252	204.566	4.543	Sy1.9	0.02297	SWIFT J1338.2+0433	
78	MAXI J1347-328	206.9	-32.9	24.8	7.1	0.3	Abell 3571	206.871	-32.866	Galaxy Cluster	0.0391	1ES 1344-32.6	
79	MAXI J1348+267	207.2	26.7	16.3	3.9	0.2	Abell 1795	207.252	26.585	Galaxy Cluster	0.062476	4U 1348+25	
80	MAXI J1349-302	207.3	-30.3	25.9	7.4	0.3	IC 4329A	207.330	-30.309	Sy1.2	0.01605	3A 1346-301	
81	MAXI J1358-480	209.7	-48.1	7.5	1.9	0.2	CIZA J1358.9-4750	209.700	-47.630	Galaxy Cluster	0.074	1RXS J135842.4-475029	
82	MAXI J1407-509	212.0	-50.9	8.5	1.9	0.2	CIZA J1407.8-5100	211.969	-51.009	Galaxy Cluster	0.0966	XSS J14080-5042	
83	MAXI J1413-031	213.3	-3.2	20.8	5.7	0.3	NGC 5506	213.312	-3.208	Sy1.9	0.00618	4U 1410-03	
84	MAXI J1418+251	214.6	25.2	12.7	3.1	0.2	NGC 5548	214.498	25.137	Sy1.5	0.01717	4U 1414+25	
85	MAXI J1429+426	217.4	42.6	8.9	2.1	0.2	1ES 1426+428	217.136	42.672	BL Lac	0.129	2MASX J14283260+4240210, 4U 1444+43	
86	MAXI J1511+058	227.9	5.9	23.1	6.1	0.3	Abell 2029	227.733	5.745	Galaxy Cluster	0.07728	3A 1509+058	
87	MAXI J1516+065	229.2	6.6	7.9	2.1	0.3	Abell 2052	229.226	6.530	Galaxy Cluster	0.035491	1ES 1514+07.2	

Table 1 (cont'd)

(1) No.	(2) MAXI Name	(3) MAXI R.A.	(4) MAXI Decl.	(5) Significance	(6) Flux <sup>a</sup>	(7) Error <sup>a</sup>	(8) Counterpart Name	(9) Ctpt. R.A.	(10) Ctpt. Decl.	(11) Type <sup>b</sup>	(12) Redshift <sup>c</sup>	(13) Other Name	(14) Note <sup>d</sup>
88	MAXI J1522+279	230.7	28.0	8.4	2.0	0.2	Abell 2065	230.678	27.723	Galaxy Cluster	0.0726	4U 1521+28	
89	MAXI J1522+084	230.7	8.4	8.4	2.0	0.2	Abell 2063	230.772	8.602	Galaxy Cluster	0.03616	1ES 1520+08.7	
90	MAXI J1558+272	239.7	27.3	21.2	5.2	0.2	Abell 2142	239.567	27.225	Galaxy Cluster	0.0909	4U 1556+27	
91	MAXI J1602+160	240.6	16.0	10.9	2.6	0.2	Abell 2147	240.572	15.895	Galaxy Cluster	0.035	4U 1601+15	
92	MAXI J1603-759	240.8	-75.9	8.5	1.5	0.2	CIZA J1601.7-7544	240.445	-75.746	Galaxy Cluster	0.153	XSS J16019-7548	
93	MAXI J1615-058	243.9	-5.8	8.8	2.3	0.3	Abell 2163	243.946	-6.146	Galaxy Cluster	0.1698	1H 1613-060	
94	MAXI J1617-283	244.5	-28.4	9.0	2.2	0.2	1RXS J161933.6-280736	244.887	-28.127	Symb/NS		SWIFT J1619.4-2808	(G)
95	MAXI J1619-156	245.0	-15.7	2976.9	19216.8	6.2	Sco X-1	244.980	-15.640	LMXB/NS		4U 1617-15	
96	MAXI J1626-335	246.7	-33.5	9.9	2.5	0.2	CIZA J1626.3-3329	246.586	-33.489	Galaxy Cluster	0.1098	XSS J16265-3303	
97	MAXI J1627-243	246.8	-24.4	11.1	2.8	0.2	3EG J1627-2419	247.000	-24.300	BL Lac	—		
98	MAXI J1628+396	247.2	39.6	16.9	4.4	0.2	Abell 2199	247.154	39.524	Galaxy Cluster	0.030151	4U 1627+39	
99	MAXI J1632-674	248.0	-67.4	83.5	21.9	0.3	KZ TrA	248.070	-67.462	LMXB		4U 1626-67, 4U 1626-673	
100	MAXI J1633+056	248.3	5.6	8.1	2.0	0.2	Abell 2204	248.194	5.571	Galaxy Cluster	0.152158	2E 1630.3+0540	
101	MAXI J1633-750	248.3	-75.0	7.8	1.3	0.2	ABELL 3628	247.755	-75.176	Galaxy Cluster	0.1492	XSS J16345-7506	
"	"	"	"	"	"	"	1RXS J163153.5-750631	247.973	-75.109	X-ray source	—		
102	MAXI J1638-643	249.6	-64.3	41.9	9.4	0.2	TrA Cluster	249.567	-64.347	Galaxy Cluster	0.0508	XSS J16384-6424	
103	MAXI J1653+398	253.4	39.8	13.2	3.2	0.2	Mrk 501	253.468	39.760	BL Lac	0.03366	4U 1651+39	
104	MAXI J1657+353	254.5	35.4	45.4	29.3	0.4	Her X-1	254.458	35.342	LMXB/NS		4U 1656+35	
105	MAXI J1701+341	255.3	34.2	9.2	2.5	0.3	Abell 2244	255.679	34.062	Galaxy Cluster	0.0968	3A 1702+340	
106	MAXI J1703+785	256.0	78.6	18.0	4.0	0.2	Abell 2256	255.931	78.718	Galaxy Cluster	0.0581	4U 1707+78	
107	MAXI J1706+241	256.7	24.1	10.0	2.3	0.2	V934 Her	256.644	23.972	LMXB/NS		4U 1700+24	
108	MAXI J1716-629	259.2	-62.9	8.8	1.6	0.2	NGC 6300	259.248	-62.821	Sy2	0.0037	SWIFT J1717.1-6249	
109	MAXI J1741+185	265.5	18.5	7.3	1.7	0.2	4C+18.51	265.530	18.456	Sy1	0.186	RX J1742.1+1827	
110	MAXI J1753-014	268.4	-1.4	130.1	64.2	0.5	SWIFT J1753.5-0127	268.368	-1.452	LMXB/ BHC			
111	MAXI J1807+061	271.9	6.1	7.7	1.9	0.2	V0426 Oph	271.966	5.862	CV/Dwarf Nova		1RXS J180751.8+055144	
112	MAXI J1815+498	274.0	49.8	31.3	8.7	0.3	AM Her	274.055	49.868	CV/AM Her		4U 1813+50, 4U 1814+50	
113	MAXI J1825-371	276.4	-37.1	76.9	32.4	0.4	V0691 CrA	276.445	-37.105	LMXB		4U 1822-371, 4U 1822-37	
114	MAXI J1826+305	276.5	30.6	7.9	1.8	0.2	CIZA J1825.3+3026	276.353	30.442	Galaxy Cluster	0.065		
115	MAXI J1835+328	278.8	32.8	11.5	2.7	0.2	3C 382	278.764	32.696	Sy1	0.05787	H 1832+325	
116	MAXI J1835-328	278.9	-32.9	23.0	7.3	0.3	XB 1832-330 (NGC 6652)	278.934	-32.991	LMXB/NS		NGC 6652	
117	MAXI J1837-653	279.5	-65.3	12.0	2.3	0.2	ESO 103-G35	279.585	-65.428	Sy2	0.01329	H 1834-653	
118	MAXI J1839+798	279.9	79.9	13.6	2.8	0.2	3C 390.3	280.538	79.771	Sy1	0.0561	4U 1847+78	
119	MAXI J1851-783	282.9	-78.3	8.5	1.5	0.2	2MASX J18470283-7831494	281.762	-78.530	Sy1	0.07412	4U 1916-79	
120	MAXI J1855-311	283.8	-31.2	21.4	6.5	0.3	V1223 Sgr	283.759	-31.163	CV/DQ Her		4U 1849-31	
121	MAXI J1900-249	285.0	-24.9	68.8	27.2	0.4	HETE J1900.1-2455	285.036	-24.921	LMXB/msPSR			
122	MAXI J1920-586	290.1	-58.6	11.8	2.5	0.2	ESO 141-G55	290.309	-58.670	Sy1	0.036	4U 1924-59	
123	MAXI J1921+439	290.3	44.0	35.5	9.7	0.3	Abell 2319	290.189	43.962	Galaxy Cluster	0.0557	4U 1919+44	
124	MAXI J1924+501	291.0	50.2	10.1	2.4	0.2	CH Cyg	291.138	50.241	Symb/WD		1RXS J192433.0+501415	
125	MAXI J1941-104	295.4	-10.4	14.1	3.8	0.3	NGC 6814	295.669	-10.323	Sy1	0.005214	2E 1939.9-1026	
"	"	"	"	"	"	"	V1432 Aql	295.048	-10.424	CV/AM Her		RX J1940.1-1025	
126	MAXI J1959+650	299.9	65.1	20.3	4.9	0.2	1ES 1959+650	299.999	65.148	BL Lac	0.047	QSO B1959+650	
127	MAXI J2009-611	302.3	-61.1	8.0	1.6	0.2	NGC 6860	302.195	-61.100	Sy1	0.01488	RX J200847-61055	
128	MAXI J2011-568	302.9	-56.9	22.0	5.2	0.2	Abell 3667	303.125	-56.816	Galaxy Cluster	0.0556	1ES 2008-57.0	
129	MAXI J2041+750	310.4	75.0	9.3	1.8	0.2	4C +74.26	310.655	75.134	Sy1	0.104	XSS J20404+7521	
130	MAXI J2044-107	311.0	-10.7	12.3	3.3	0.3	Mrk 509	311.041	-10.723	Sy1.2	0.0344	3A 2041-107	

Table 1 (cont'd)

(1)	(2)	(3)	(4)	(5)	(6)	(7)	(8)	(9)	(10)	(11)	(12)	(13)	(14)
No.	MAXI Name	MAXI R.A.	MAXI Decl.	Significance	Flux <sup>a</sup>	Error <sup>a</sup>	Counterpart Name	Ctpt. R.A.	Ctpt. Decl.	Type <sup>b</sup>	Redshift <sup>c</sup>	Other Name	Note <sup>d</sup>
131	MAXI J2129+121	322.5	12.2	42.7	12.2	0.3	4U 2129+12	322.493	12.167	LMXB in globular clus		4U 2127+119	
132	MAXI J2135-626	323.8	-62.7	7.4	1.5	0.2	1RXS J213623.1-622400	324.096	-62.400	Sy1	0.0588	6dFGS gJ213623.1-622401	
133	MAXI J2144+383	326.2	38.3	550.6	702.3	1.2	Cyg X-2	326.172	38.322	LMXB/NS		4U 2142+38	
134	MAXI J2201-600	330.3	-60.1	8.3	1.7	0.2	Abell 3827	330.483	-59.949	Galaxy Cluster	0.0984	1RXS J220157.8-595648	
135	MAXI J2202-319	330.6	-31.9	7.6	2.0	0.3	NGC 7172	330.508	-31.870	Sy2	0.00868	SWIFT J2201.8-3152	
136	MAXI J2214+125	333.6	12.6	7.2	1.7	0.2	RU Peg	333.511	12.703	CV/Dwarf Nova		2E 2211.5+1227	
137	MAXI J2218-084	334.6	-8.4	12.5	3.3	0.3	FO Aqr	334.481	-8.351	CV/DQ Her		2E 2215.3-0835	
138	MAXI J2235-259	339.0	-25.9	9.3	2.5	0.2	NGC 7314	338.943	-26.050	Sy1.9	0.00476	3A 2233-259	
139	MAXI J2253+163	343.5	16.3	17.0	4.4	0.3	3C 454.3	343.491	16.148	Blazar	0.859	1E 2251.5+1553	
140	MAXI J2253-177	343.5	-17.7	11.8	3.0	0.2	MR 2251-178	343.524	-17.582	Sy1	0.06398	2A 2251-179	
141	MAXI J2255-031	343.8	-3.1	12.7	3.4	0.3	AO Psc	343.825	-3.178	CV/DQ Her		3A 2253-033	
142	MAXI J2305-085	346.3	-8.6	14.8	3.9	0.3	Mrk 926	346.181	-8.686	Sy1.5	0.04686	4U 2305-07	
143	MAXI J2316-425	349.1	-42.6	7.1	2.0	0.3	Abell S1101	348.494	-42.727	Galaxy Cluster	0.058	1E 2311.2-4259	

<sup>a</sup>The flux is in units of  $10^{-11}$  ergs cm<sup>-2</sup> s<sup>-1</sup> in the 4-10 keV band, converted from Crab units; 1 Crab =  $1.21 \times 10^{-8}$  ergs cm<sup>-2</sup> s<sup>-1</sup>.

<sup>b</sup>Sy: Seyfert galaxy, LMXB: low-mass X-ray binary, HMXB: high-mass X-ray binary, Symb: symbiotic star, NS: neutron star, BHC: black hole candidate, CV: cataclysmic variable, ULX: ultra-luminous X-ray source, msPSR: millisecond pulsar.

<sup>c</sup>The redshifts are taken from the online database SIMBAD and NED. A blank indicates the source is Galactic, and — indicates the source has no redshift information.

<sup>d</sup>(A) Identified by individual inspection since in the image fitting the position is unable to be determined due to significant source confusion with Perseus Cluster. (B) The data is extended compared with the PSF model. (C) Matsumura et al.(2011) (D)Suzuki et al.(2010) (E) Isobe et al.(2010) (F) This source is likely to be contaminated by 1RXS J133344.4-231734 and TV Hya. ESO 509-IG66 has double nuclei with similar fluxes in the 2-10 keV band (Guainazzi et al. 2005). The redshift is adopted from Sekiguchi & Wolstencroft (1992). (G) This source is possibly contaminated by V893 Sco and other nearby sources.